The study of Nuclear Mass Model by Sequential Least Squares Programming*

Hang Yang,[1] Cunyu Chen,[1] Xiaoyu Xu,[1] Hankui Wang,[1,†] and Youbao Wang[2,‡]

[1]*School of Science, Zhejiang Sci-Tech University, Hangzhou 310018, China*
[2]*China Institute of Atomic Energy, P.O. Box 275(10), Beijing 102413, China*

Nuclear mass is an important property in both nuclear and astrophysics. In this work, we explore the improved mass model incorporating a higher-order term of the symmetry energy through some algorithms. The Sequential Least Squares Programming (SLSQP) algorithm augments the precision of this multinomial mass model by diminishing the error from 1.863 MeV to 1.631 MeV. These algorithms are further examined by utilizing 200 sample mass formulas devised from the δE term of the $E_{isospin}$ mass model. The SLSQP method exhibits superior performance compared to the other algorithms in terms of errors and convergence speed. This algorithm proves to be more advantageous for handling large-scale, multi-parameter optimization tasks in nuclear physics.

Keywords: Nuclear mass model, binding energy, magic nuclei, sequential least squares algorithm

I. INTRODUCTION

An atomic nucleus, which contains valuable information about the atomic structure, is a fundamental physical property [1]. Changes in atomic mass directly affect nuclear stability and energy release during nuclear reactions [2]. The mass of a neutron-rich nucleus plays a crucial role in fast neutron capture (r-process) during stellar nucleosynthesis. Thus, studying the mass is essential for a comprehensive understanding of the formation and evolution of elements in the universe [3–5]. Recently, the development of radioactive ion beam facilities has led to experimental measurements of over 3000 ground state atomic masses [6, 7], with the study continuously expanding to both sides of the β-stability line. In astrophysics, large amounts of data regarding the masses of neutron-rich or neutron-poor nuclei in regions far from the stability line are required. This is difficult to measure directly using current technology. Therefore, many different types of mass models have been proposed.

In 1935, Bethe-Weizsacker proposed the semiempirical BW2 mass formula [8–10] that predicts mass with an accuracy of approximately 3 MeV. In Ref.[11], nuclear binding energy is divided into two parts: a large and smooth component along with a small and fluctuating component. The classical droplet model only accounts for the smooth trend, failing to consider the rapid fluctuation of the binding energy around the shell gap with a number of protons and neutrons. This suggests that important physical effects are absent in the classical mass model [12, 13]. To solve this problem, physicists have developed macroscopic-microscopic mass models. These models introduce shell correction terms, such as the finite force range droplet model (FRDM) [14], Koura-Tachibana-Uno-Yamada (KTUY) [15], Lublin Strasbourg drop (LSD) [16], and micromass models such as the Hartree-Fock-Bogoliubov (HFB) approach [17, 18] and relativistic mean-field theory (RMF) [19]. The cited research is primarily based on the density functional theory (DFT) [20]. Although DFT is more complex, it exhibits superior extrapolation capabilities.

Kirson et al. added six physical terms as constraints to the mass model [21–27]. The BW2 mass model thus obtained was improved to some extent, addressing the problems of missing physics and overfitting that existed in early semi-empirical mass formulations, thereby reducing the root mean square error (RMSD) [28] to 1.92 MeV. Machine learning has important applications in nuclear physics because of its ability to handle complex problems, such as predicting half-life, charge radius, and charge density [29–32]. By considering the α-decay energy and Garvey-Kelson relations (GKs) and applying the multi-objective optimization (MOO) method [13, 33, 34], Qian and his research team significantly improved the theoretical accuracy of the BW2 model. Taking into account the isospin dependence, Bhagwat improved the liquid drop model to a model related to isospin and added fluctuation terms [35], which explained the binding energy of nucleons very well. The sequential least squares programming [36] is a suitable algorithm for solving nonlinear optimization problems with constraints, as it can handle multiple constraints and nonlinear objective functions.

In this work, we study the improved BW2 mass model with a higher-order term of the symmetry energy [37] by employing certain algorithms such as SLSQP. The mass models and algorithms are presented in Part II. In Part III, we test the generality of the SLSQP method using 200 sample mass formulas that are derived from randomly selected parameters of the $E_{isospin}$ mass model. The conclusions are provided in Part IV.

II. SEMI-EMPIRICAL MASS FORMULA

A. BW3 Mass model

The mass model of BW3 is derived from the droplet model and improves the semi-empirical mass formula [8–10] by in-

* The research at ZSTU was supported by the National Natural Science Foundation of China (Grants No.U2267205, No.12475124), a ZSTU intramural grant(22062267-Y), and Excellent Graduate Thesis Cultivation Fund (LW-YP2024011).

† Corresponding author,Hankui Wang, whk2007@163.com
‡ Corresponding author,Youbao Wang, ybwang@ciae.ac.cn

corporating additional physical constraints [37]:

$$\begin{aligned} B_{BW3} &= \alpha_V A + \alpha_S A^{2/3} + \alpha_C \frac{Z^2}{A^{1/3}} + \alpha_t \frac{(N-Z)^2}{A} \\ &+\alpha_{xC} \frac{Z^{4/3}}{A^{1/3}} + \alpha_W \frac{|N-Z|}{A} + \alpha_{st} \frac{(Z-N)^2}{A^{4/3}} \\ &+\alpha_p \delta(N,Z) A^{-1/2} + \alpha_R A^{1/3} + \alpha_m P + \beta_m P^2 \\ &+\alpha_{pm} \frac{(N-Z)^4}{A^3}. \end{aligned} \quad (1)$$

Eq.(1) involves 12 parameters, and the $\delta(N,Z)$ is defined as:

$$\delta(N,Z) = [(-1)^N + (-1)^Z]/2, \quad (2)$$

where 1 denotes even-even nuclei, -1 odd-odd nuclei, and 0 odd-A nuclei. P can be expressed as follows:

$$P = \frac{v_p v_n}{v_p + v_n}. \quad (3)$$

Here v_p (v_n) represents the difference between Z (N) and the magic number nearby.

$$\alpha_{pm} = \frac{1}{162} \left(\frac{9\pi}{8}\right)^{\frac{2}{3}} \frac{\hbar^2}{m r_0^2}. \quad (4)$$

Eq.(4) and its physical terms are derived from the application of the Fermi gas model to account for the nucleon binding energies. Following the restrictions of Pauli's exclusion principle, the nucleons (protons, neutrons, and nuclei) are assumed to move freely within the nuclear volume. The potential experienced by each nucleon is a superposition of the potentials created by other nucleons. The Fermi gas model gives the total kinetic energy of the nucleons as follows:

$$\begin{aligned} \langle E(Z,N) \rangle &= N\langle E_N \rangle + Z\langle E_Z \rangle \\ &= \frac{3}{10m} \frac{\hbar^2}{r_0^2} \left(\frac{9\pi}{4}\right)^{\frac{2}{3}} \left(\frac{N^{\frac{5}{3}} + Z^{\frac{5}{3}}}{A^{\frac{2}{3}}}\right). \end{aligned} \quad (5)$$

Assuming that the radii of the proton and neutron potential wells are identical, a binomial expansion near $N = Z$ yields the following expression:

$$\begin{aligned} \langle E(Z,N) \rangle &= \frac{3}{10m} \frac{\hbar^2}{r_0^2} \left(\frac{9\pi}{8}\right)^{\frac{2}{3}} [A + \frac{5}{9} \frac{(N-Z)^2}{A} \\ &+\frac{5}{243} \frac{(N-Z)^4}{A^3} + \cdots]. \end{aligned} \quad (6)$$

The first term contributes to the volume in the mass formula, whereas the second corrects for $N \neq Z$. The third term represents the higher-order addition to the symmetry energy used to enhance the mass model.

B. $E_{isospin}$ Mass model

The $E_{isospin}$ mass formula can be expressed by Strutinsky's theorem [35]:

$$E_{isospin}(Z,N) = -(E_{LDM} + \delta E). \quad (7)$$

Here, E_{LDM} represents the Macroscopic (M) section, which contains 9 free parameters, hereinafter referred to as M-parameters. The δE term corresponds to the Fluctuation (F) of the binding energy and can generate over 100 parameters, which are hereinafter referred to as F-parameters. These F-parameters can be set as the parameter pool to form sample mass formulae to test the generality of these algorithms.

The macroscopic section includes the volume term related to the isotopic spin, the Coulomb term, the surface term, the Coulomb energy correction term related to surface diffusion and the pairing term:

$$\begin{aligned} E_{LDM} &= \alpha_V \left[1 + \frac{4k_V T_z(T_z+1)}{A^2}\right] A \\ &+\alpha_S \left[1 + \frac{4k_S T_z(T_z+1)}{A^2}\right] A^{2/3} \\ &+\frac{3Z^2 e^2}{5 r_0 A^{1/3}} + \frac{\alpha_C Z^2}{A} + E_p. \end{aligned} \quad (8)$$

Here, a_V, k_V, a_S, k_S, a_C, and r_0 represent volume energy, isospin dependence of volume energy, surface energy, isospin dependence of surface energy, Coulomb energy, and Coulomb radius, respectively. T_Z is the third component of the isospin, and e is the electron charge. As correcting, the smooth pairing energy [38] is given as:

$$E_p = \begin{cases} \frac{\lambda_n}{N^{1/3}}, & Z \text{ even}, \ N \text{ odd}, \\ \frac{\lambda_p}{N^{1/3}}, & Z \text{ odd}, \ N \text{ even}, \\ \frac{\lambda_n}{N^{1/3}} + \frac{\lambda_p}{N^{1/3}} + \frac{\lambda_{np}}{N^{1/3}}, & Z, N \text{ odd}, \\ 0, & N, Z \text{ even}. \end{cases} \quad (9)$$

Here λ_n, λ_p, and λ_{np} are free parameters. The smooth pairing energy of even-even nuclei is zero, because both protons and neutrons pair well in even-even nuclei.

The δE can be expressed as:

$$\begin{aligned} \delta E(\vec{x}) = \sum_{\vec{k}=\vec{0}}^{\vec{M}} \Big\{ & a_{\vec{k}} \cos\left(2\pi \frac{\vec{x}\cdot\vec{k}}{M}\right) \\ &+ b_{\vec{k}} \sin\left(2\pi \frac{\vec{x}\cdot\vec{k}}{M}\right) \Big\}. \end{aligned} \quad (10)$$

Here $\vec{k} \equiv (k_1, k_2, k_3, k_4)$ ($0 \leq k_i \leq M$ for $i = 1, 2, 3, 4.$), and $\vec{x} \equiv (x_1, x_2, x_3, x_4)$:

$$\begin{aligned} x_1 = \beta_1 \left|\tfrac{N-N_o}{N}\right|, \quad x_2 = \beta_2 \left|\tfrac{Z-Z_o}{Z}\right|, \\ x_3 = \beta_3 N^{1/3}, \quad x_4 = \beta_4 Z^{1/3}. \end{aligned} \quad (11)$$

In this formula, $N_0(Z_0)$ is the magic number nearby. The β_1, β_2, β_3, and β_4 are the free parameters. The β_1 and β_2 describe the closeness to a shell closure given proton and neutron conditions, and β_3, and β_4 are proportional to Fermi momentum. The number of such parameters becomes quite large $(2M^4 + 4)$, while not all terms need to be expanded to M. so it can be simplified as:

$$\begin{aligned} \delta E(\vec{x}) = & \sum_{k_1=0}^{M} \sum_{k_2=0}^{M-k_1} \sum_{k_3=0}^{M-k_1-k_2} \sum_{k_4=0}^{M-k_1-k_2-k_3} \\ & \left\{ a_{\vec{k}} \cos\left(2\pi \frac{\vec{x}\cdot\vec{k}}{M}\right) + b_{\vec{k}} \sin\left(2\pi \frac{\vec{x}\cdot\vec{k}}{M}\right) \right\}. \end{aligned} \quad (12)$$

It reduces the number of parameters to $\frac{1}{12}(M+4)!/M!+4$. Since the mean of δE is almost 0. Therefore, the free parameter can be further reduced to $\frac{1}{12}(M+4)!/M!+2$.

C. Algorithm Principles

This work studies some algorithms, namely Ordinary Least Squares (OLS) [39], SLSQP [36], Constrained Optimization by Linear Approximation (COBYLA) [40], Broyden-Fletcher-Goldfarb-Shanno (BFGS) [41], Conjugate Gradient (CG) [42], and so on. SLSQP, COBYLA, and Trust-Constr [43] were found to be better effective algorithms for solving constrained optimization problems (COPs). For solving the COP in Eq.(9), SLSQP was used because only SLSQP utilizes the information in the gradient and Hessian matrix [44] to the fullest extent, resulting in faster convergence to the optimal solution.

$$\begin{aligned} \min \quad & f(\vec{x}) \\ st \quad & g(\vec{x})=0, h(\vec{x})\geq 0 \\ where \quad & \vec{x}=(x_1,x_2,x_3,\ldots,x_{k-2},x_{k-1},x_k)\in X \\ & X=\vec{x}|\vec{l}\leq\vec{x}\leq\vec{u} \\ & \vec{l}=(l_1,l_2,l_3,\ldots,l_{i-2},l_{i-1},l_i) \\ & \vec{u}=(u_1,u_2,u_3,\ldots,u_{j-2},u_{j-1},u_j). \end{aligned} \tag{13}$$

In this formula, $\vec{x}$ is the solution vector, X is the vector space of solution vectors, $\vec{l}$ ($\vec{u}$) is the upper (lower) bounds of the solution vector space, $g(\vec{x})$ is the equality constraint, $h(\vec{x})$ is the inequality constraint, and $f(\vec{x})$ is the objective optimization function [45].

The SLSQP algorithm iteratively minimizes the objective function under constraints through linear approximation. This transforms the nonlinear constrained problem into an unconstrained least squares problem. In each iteration, the gradient and Hessian matrix [44] are calculated to update the solution using Lagrange multipliers for the constraints.

$$L(\vec{x},\vec{\lambda},\vec{\mu})=f(\vec{x})+\vec{\lambda}^T*g(\vec{x})+\vec{\mu}^T*h(\vec{x}). \tag{14}$$

The superscript T denotes the transpose of the vector, $\vec{\lambda}$ and $\vec{\mu}$ represent the penalty terms associated with the equality and inequality conditions, respectively [46].

By solving the unconstrained least squares problem, an update rule is obtained for each iteration. This rule satisfies not only the equality and inequality constraints but also the first-order necessary conditions:

$$\nabla L(\vec{x},\vec{\lambda},\vec{\mu})=\nabla f(\vec{x})+J_g^T*\vec{\lambda}+J_h^T*\vec{\mu}=0, \tag{15}$$

J_g and J_h denote the Jacobian matrices of the equality and inequality constraints, respectively [47].

According to the above update rule, the initial value $\vec{x}_1$ is chosen and the stopping criterion ε is set. The gradient vector $\nabla f_k(\vec{x}_k)$ is computed at each iteration k. If $||\nabla f_k(\vec{x}_k)||<\varepsilon$, the algorithm is terminated, obtaining an approximate solution $\vec{x}^*$. This process constructs a sequential programming model as follows:

$$\begin{aligned} \min \quad & q(\vec{x})=f_k(\vec{x})+g_k^T(\vec{x}-\vec{x}_k) \\ & \qquad +\frac{1}{2}(\vec{x}-\vec{x}_k)^T B_k(\vec{x}-\vec{x}_k) \\ st \quad & A_{eq}(\vec{x}-\vec{x}_0)=0 \\ & g_k(\vec{x})\geq 0, k=1,2,\ldots,k. \end{aligned} \tag{16}$$

In this formula B_k is a positive definite symmetric matrix used to approximate the inverse of the Hessian matrix, and A_{eq} is the Jacobian matrix of the equality constraints.

This model is solved to obtain the modified direction $\Delta\vec{x}$, computing the step size α such that the objective function sufficiently decreases along the search direction:

$$\begin{aligned} \alpha &= \min(1,r) \\ r &= \max(\beta_s,r_t) \\ \beta_s &= \left(\frac{\partial f}{\partial\vec{x}}\right)^T(\Delta\vec{x}/s) \\ r_t &= \left(\frac{\partial g}{\partial\vec{x}}\right)^T(\Delta\vec{x}/t), \end{aligned} \tag{17}$$

where s and t are positive scale factors. Finally, the estimated points are updated as follows: $\vec{x}_{k+1}=\vec{x}_k+\alpha\Delta\vec{x}$. By solving the above system of equations following this iterative process, the objective function is gradually optimized to determine the optimal solution that satisfies the constraints.

III. DISCUSSION

The coefficients of BW3 model are improved with less error between the calculated values and the experimental data by using SLSQP algorithm [36]. Subsequently, the following constraints are incorporated to guarantee the physical viability of the program calculations:

1. The nuclide numbers should satisfy $N\geq 8$ and $Z\geq 8$.
2. After satisfying Condition 1, the specific binding energy of the remaining nuclides, $\frac{B_{Th}}{N+Z}$, is distributed in the range of 5 - 9 MeV.

The performance metrics of the model were evaluated using RMSD [28], which is defined as follows:

$$RMSD=\sqrt{\frac{\sum_{i=1}^{n}(B_{Ex_i}-B_{Th_i})^2}{n}}, \tag{18}$$

where n represents the total number of nuclides involved in the calculation; B_{Ex_i} and B_{Th_i} are the current experimental and theoretical nuclide binding energies, respectively.

The modified coefficients corresponding to several algorithms are listed in Table 1. The different algorithms can lead to alterations in the weights of the terms within the model, as shown in the table. The weights signify the degree to which each term affects the model, and the symbols denote positive or negative corrections. The volume, surface, symmetry,

TABLE 1. Coefficients of the BW3 mass model under each algorithm for binding energy (in MeV)

	OLS	SLSQP	BFGS	Trust-Constr	L-BFGS-B	CG
α_V	16.58	16.05	16.05	16.03	15.19	16.20
α_S	-26.95	-23.10	-23.10	-22.96	-16.47	-23.33
α_C	-0.774	- 0.74	- 0.74	- 0.74	- 0.71	-0.74
α_t	-31.51	-31.62	-31.62	-31.53	-25.83	-31.50
α_{xC}	2.22	1.59	1.59	1.59	1.42	1.39
α_W	-43.40	-72.96	-72.97	-72.14	5.39	-57.06
α_{st}	55.62	64.10	64.10	63.59	23.84	54.80
α_p	9.87	10.56	10.56	10.56	12.36	10.63
α_R	14.77	9.89	9.89	9.64	- 4.19	9.87
α_m	- 1.90	- 1.88	- 1.88	- 1.88	- 1.82	-1.89
β_m	0.14	0.14	0.14	0.14	0.14	0.14
α_{pm}	- 1.30	-11.36	-11.36	-11.31	- 1.13	0.14

Wigner, surface symmetry, pairing, higher-order correction, and curvature terms possess high weights due to their significant influence on the mass model, whereas the Coulomb, Coulomb exchange, and shell effect terms [21–27] carry low weights because of their relatively minor influence. In the plot, the horizontal coordinate represents the number of neutrons N, and the vertical coordinate represents the percentage of relative error [12], which is defined as

$$\frac{\delta B}{B}(\%) = \frac{B_{Ex} - B_{Th}}{B_{Ex}} * 100\%. \tag{19}$$

The errors exhibit different trends for different nuclide regions under different algorithms. Figs.1-a, 1-b, and 1-c show the reduction in the overall error and narrowing in the fluctuation range of the light and medium nuclide regions. In Figs.1-e and 1-f, the fluctuation amplitude of the heavy nuclide regions increases, which leads to an increase in the fluctuation amplitude of the light nuclide regions, such that the total RMSD does not decrease or even deteriorate. SLSQP [36] exhibits greater advantages in reducing model errors when comparing performance metrics such as $\frac{\delta B}{B}(\%)$ [12] and RMSD [28] of the mass model obtained using different algorithms. This is attributed to the reduced weights of the surface and curvature terms by SLSQP and increased weights of Wigner, surface symmetry, pairing, and higher-order correction terms. The results also show that in AME2020, the influence of the surface and curvature terms on the binding energy decreases, while that of the Wigner, surface symmetry, pairing, and higher-order correction terms on the overall effect increases. This also indicates that the mass model under SLSQP not only reduces the impact of the surface and curvature terms on the binding energy but also enhances the impact of the Wigner term on the overall effect, thereby improving its extrapolation ability [17, 18] and more accurately reflecting the contributions of different physical terms to binding energy.

Fig.2 shows the relative error between the theoretical and experimental values of the BW3 mass model obtained by employing the SLSQP and OLS algorithms, where the x-axis represents the neutron number, the y-axis stands for the atomic number, and the z-axis corresponds to the relative error percentage $\frac{\delta B}{B}(\%)$. In the figure, the fluctuations in differences are more pronounced for the magic nuclei, particularly those nuclei in the vicinity of the doubly magic nuclei, which implies distinct interactions between magic and non-magic nuclei. The SLSQP improves the error near the doubly magic nuclei, captures the special interaction effects around the magic nuclei more accurately, and thus enhances the accuracy of the theoretical model.

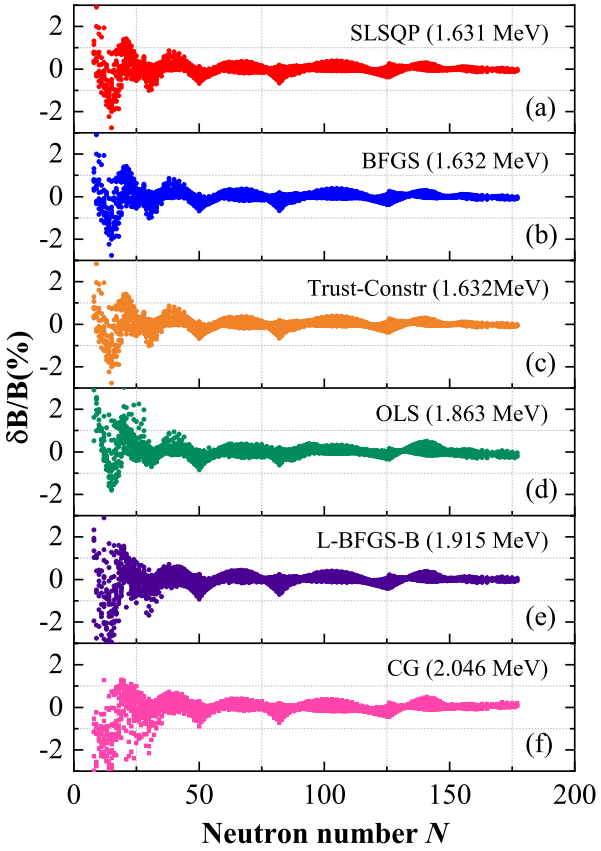

Fig. 1. BW3 mass model relative error comparison using different algorithms, and its RMSD is shown in parentheses.

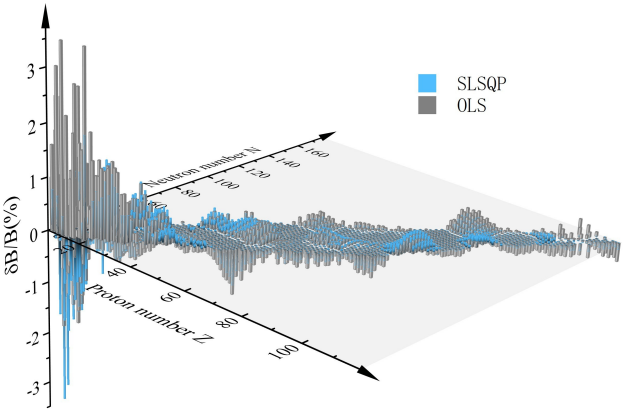

Fig. 2. BW3 mass model relative error comparison with SLSQP/OLS coefficients.

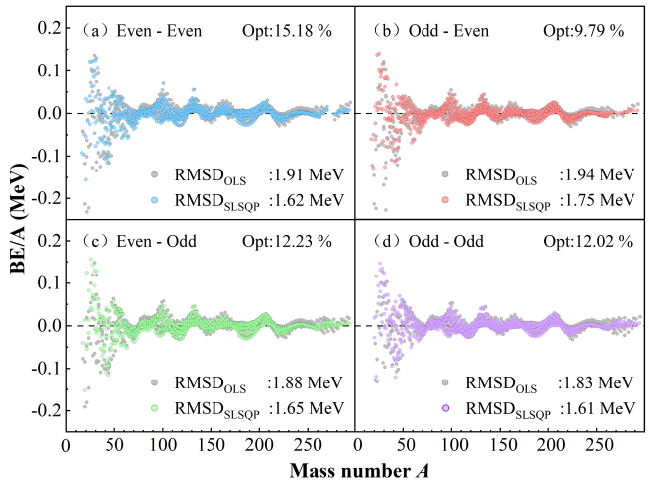

Fig. 3. BW3 mass model performance on total nuclei with SLSQP/OLS coefficients.

Fig.3 shows the performance of the SLSQP with regard to even-even, odd-odd, and odd-A nuclei. The optimization effect of SLSQP on the different types of nuclei shows significant differences. The improvement is most pronounced for even-even nuclei, while certain optimization results can also be attained for odd-A and odd-odd nuclei. Fig.3-a shows that for even-even nuclei [48] (both Z and N are even), the SLSQP provides a significant reduction in RMSD [28] by 0.29 MeV, with a performance improvement of about 15.18%, achieving a more substantial optimization in the whole nuclei region compared with the theoretical value of the BW3 model with OLS coefficients. In Fig.3-b, for odd-Z and even-N nuclei, after the SLSQP optimization, the model RMSD is reduced by 0.19 MeV, with a performance improvement of approximately 9.79%. Similarly, in Fig.3-c, for even-Z and odd-N nuclei, the model RMSD is reduced by 0.23 MeV, with a performance improvement of approximately 12.23%. Notably, in the medium-nuclei region, the optimization results are closer to the experimental values. For odd-odd nuclei (both Z and N are odd), Fig.3-d shows that after SLSQP optimization, the model RMSD is reduced by 0.22 MeV and performance is improved by approximately 12.02%. Particularly, in the heavy nuclei region, the optimization results are closer to the experimental values. These results further validate the effectiveness of the SLSQP in this mass model optimization.

To test the generality of the SLSQP method, we devise 200 sample mass formulas by randomly selecting parameters from the F-parameters in the δE term of the $E_{isospin}$ mass model. As mentioned before, the $E_{isospin}$ mass model consists of two parts: the E_{LDM} term, which contains 9 M-parameters derived from the liquid drop model, and the δE term, which encompasses more than 100 F-parameters. If we set M = 4 in the $E_{isospin}$ mass model, it will yield 144 F-parameters. Subsequently, we compare the results with the nuclear mass dataset AME2020, and find that the RMSD is 1.268 MeV in this situation. Next, we test the contributions of these F-parameters one by one and identify 53 of them that have obvious effects on the binding energy. After that, we randomly select 10 F-parameters from the 53 F-parameters and combine them with the 9 M-parameters to form a sample mass formula. In this manner, we devise 200 sample mass formulas to test the algorithms presented in this work. It turns out that the SLSQP method outperforms the other algorithms in terms of both errors and convergence speed.

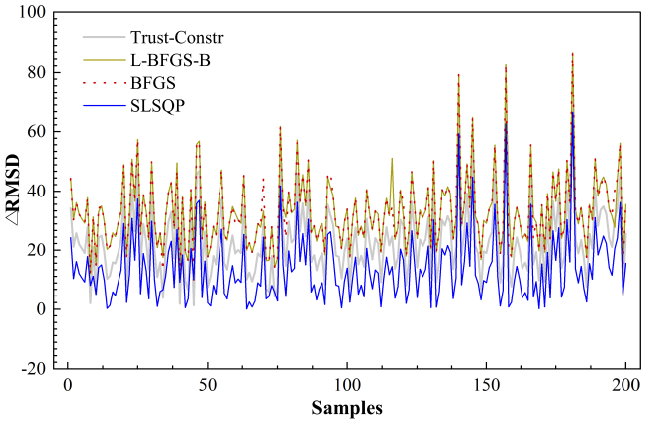

Fig. 4. Finding 62 important parameters from the δE term of $E_{isospin}$ mass model, randomly selecting 10 items as a sample formula with E_{LDM}, and obtaining 200 samples of mass formulas. The $\triangle RMSD$ is defined as $(RMSD - RMSD_{min}) * 100$, where $RMSD_{min}$ is the minimum root mean square deviation optimized by the algorithm for 200 samples.

As shown in Fig.4, the SLSQP performs significantly better than the BFGS and L-BFGS-B algorithms. For example, at the 48th sample point, the $\triangle RMSD$ of the SLSQP is 4 MeV, while that of BFGS and L-BFGS-B are 23.9 MeV and 23.0 MeV respectively. At the 67th sample point, the $\triangle RMSD$ of SLSQP is 2.7 MeV, while that of the BFGS and L-BFGS-B are 22.7 MeV and 21.8 MeV respectively. As for the Trust-Constr algorithm, it exhibits a large error amplitude, which results in poor stability during parameter optimization. In terms of computational efficiency, compared with the SLSQP algorithm as a reference, the BFGS takes approximately 2.44 times longer, the L-BFGS-B takes around 2.78 times longer, and the Trust-Constr takes a staggering 8.44 times longer. The SLSQP algorithm not only has good stability with small root mean square errors but also high computational efficiency.

To verify the effectiveness of the SLSQP, a comparison between experimental and theoretical values was carried out, as illustrated in Fig.5. The experimental binding energy (BE) values were sourced from the AME2020, whereas the theoretical values were obtained by optimizing the BW3 mass model using the SLSQP. Among the experimental values, the maximum BE for O isotopes is currently measured at $^{24}O_{16}$ with a BE value of 168.95 MeV. Beyond this isotope, the BE decreases as the N increases. The SLSQP-optimized theoretical model predicts the maximum point to be at $^{26}O_{18}$ with a BE value of 168.95 MeV, followed by a similar decline in BE with the increase in N. For the other isotope chains, the experimental BE values exhibit an overall increas-

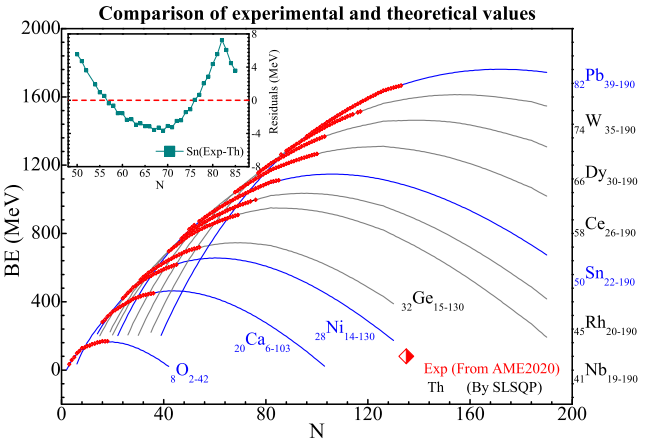

Fig. 5. Binding energy of Exp from the AME2020 [6, 7], and the theoretical predicted value by SLSQP method.

ing trend without reaching a maximum point. By optimizing the BW3 nuclear mass model through the SLSQP method, the following maximum BE points are predicted for these isotope chains: $^{64}Ca_{44}$ = 464.33 MeV, $^{88}Ni_{60}$ = 656.72 MeV, $^{123}Nb_{82}$ = 950.29 MeV, $^{141}Rh_{96}$ = 1035.66 MeV, $^{100}Ge_{68}$ = 745.77 MeV, $^{156}Sn_{106}$ = 1148.31 MeV, $^{184}Ce_{126}$ = 1311.84 MeV, $^{206}Dy_{140}$ = 1463.63 MeV, $^{230}W_{156}$ = 1613.36 MeV, $^{252}Pb_{170}$ = 1761.89 MeV.

IV. CONCLUSIONS

In this work, we investigate the improved mass model with a higher-order term of the symmetry energy by employing several algorithms. The SLSQP algorithm demonstrates the best performance in terms of both root mean square errors and computational efficiency. This algorithm reduces the global RMSD from 1.863 MeV to 1.631 MeV (12.45% reduction). The odd (even) number of protons and neutrons are discussed, and the SLSQP reduces the local RMSD from 1.91 MeV to 1.62 MeV (15.18% optimization), when nuclei have even numbers in both protons and neutrons. The local RMSD is reduced from 1.83 MeV to 1.61 MeV, when nuclei have odd numbers in both protons and neutrons. With odd (even) number of protons (neutrons), the local RMSD is reduced from 1.94 MeV to 1.75 MeV (9.79% optimization). The local RMSD is reduced from 1.88 MeV to 1.65 MeV (12.23% optimization), when proton number is even and neutron is odd. We test these algorithms using 200 sample mass formulas devised from the $E_{isospin}$ mass model. Each sample mass formula includes 19 free parameters, among which 9 are M-parameters derived from the liquid drop model, and 10 are F-parameters from the δE term of the $E_{isospin}$ mass model. The SLSQP method provides better performance than the other algorithms in errors and convergence speed. According to this work, the SLSQP algorithm is suitable for handling large-scale, multi-parameter optimization tasks in nuclear physics.

[1] B. Michael, P. H. Heenen, P. G. Reinhard, Self-consistent mean-field models for nuclear structure. Rev. Mod. Phys **75**, 121-180 (2003). https://doi.org/10.1103/RevModPhys.75.121

[2] D. Lunney, J. M. Pearson, and C. Thibault, Recent trends in the determination of nuclear masses. Rev. Mod. Phys **75**, 1021-1082 (2003). https://doi.org/10.1103/RevModPhys.75.1021

[3] A. C. Larsen, A. Spyrou, S. N. Liddick et al., Novel Techniques for Constraining Neutron-Capture Rates Relevant for r -Process Heavy-Element Nucleosynthesis. Prog. Part. Nucl. Phys **107**, 69-108 (2019). https://doi.org/10.1016/j.ppnp.2019.04.002

[4] T. Yamaguchi, H. Koura, M. Wang et al., Masses of exotic nuclei. Prog. Part. Nucl. Phys **120**, 103882 (2021). https://doi.org/10.1016/j.ppnp.2021.103882

[5] J. Erler, N. Birge, M. Kortelainen et al., The limits of the nuclear landscape. Nature **486**, 509-512 (2012). https://doi.org/10.1038/nature11188

[6] W. J. Huang, M. Wang, F. G. Kobdev et al., The AME 2020 atomic mass evaluation (I). Evaluation of input data, and adjustment procedures. Chinese. Phys. C **45**, 030002 (2021). https://doi.org/10.1088/1674-1137/abddb0

[7] M. Wang, W. J. Huang, F. G. Kobdev et al., The AME 2020 atomic mass evaluation (II). Tables, graphs and references. Chinese. Phys. C **45**, 030003 (2021). https://doi.org/10.1088/1674-1137/abddaf

[8] P. Möller, A. J. Sierk, T. Ichikawa et al., Nuclear ground-state masses and deformations: FRDM(2012). At. Data Nucl. Data Tables **109-110**, 1-204 (2016). https://doi.org/10.1016/j.adt.2015.10.002

[9] C. F. v. Weizsäcker, Leipzig, Zur Theorie der Kernmassen. Z. Physik **96**, 431-458 (1935). https://doi.org/10.1007/BF01337700

[10] H. A. Bethe, R. F. Bacher, Nuclear Physics A. Stationary States of Nuclei. Rev. Mod. Phys **8**, 82 (1936). https://doi.org/10.1103/RevModPhys.8.82

[11] B. Mohammed-Azizi, Better insight into the Strutinsky method. Phys. Rev. C **100**, 034319 (2019). https://doi.org/10.1103/PhysRevC.100.034319

[12] D. Benzaid, S. Bentridi, A. Kerraci et al., Bethe-Weizsacker semiempirical mass formula coefficients 2019 update based on AME2016. Nucl. Sci. Tech **31**, 9 (2020). https://doi.org/10.1007/s41365-019-0718-8

[13] W. H. Ye, Y. B. Qian, Z. Z. Ren, Accuracy versus predictive power in nuclear mass tabulations. Phys. Rev. C **106**, 024318 (2022). https://doi.org/10.1103/PhysRevC.106.024318

[14] P. Möller, W. D. Myers, H. Sagawa et al., New Finite-Range Droplet Mass Model and Equation-of-State Parameters. Phys. Rev. Lett **108**, 052501 (2012). https://doi.org/10.1103/PhysRevLett.108.052501

[15] H. Koura, T. Tachibana, M. Uno et al., Nuclidic Mass Formula on a Spherical Basis with an Improved Even-Odd Term. Prog. Theor. Phys **113**, 305 (2005). https://doi.org/10.1143/PTP.113.305

[16] F. A. Ivanyuk, K. Pomorski,Optimal shapes and fission barriers of nuclei within the liquid drop model. Phys. Rev. C **79**, 054327 (2009). https://doi.org/10.1103/PhysRevC.79.054327

[17] S. Goriely, N. Chamel, J. M. Pearson,Further explorations of Skyrme-Hartree-Fock-Bogoliubov mass formulas. XII. Stiff-

ness and stability of neutron-star matter. Phys. Rev. C **82**, 035804 (2010). https://doi.org/10.1103/PhysRevC.82.035804
[18] S. Goriely, N. Chamel, Further explorations of Skyrme-Hartree-Fock-Bogoliubov mass formulas. XIII. The 2012 atomic mass evaluation and the symmetry coefficient. Phys. Rev. C **88**, 024308 (2013). https://doi.org/10.1103/PhysRevC.88.024308
[19] R. A. Rego, Mean free path in the relativistic mean field. Phys. Rev. C **44**, 1944 (1991). https://doi.org/10.1103/PhysRevC.44.1944
[20] J. L. Janssen, Y. Gillet, A. Martin et al., Precise effective masses from density functional perturbation theory. Phys. Rev. B **93**, 205147 (2016). https://doi.org/10.1103/PhysRevB.93.205147
[21] W. K. Michael, Mutual influence of terms in a semi-empirical mass formula. Nucl. Phys. A. **798**, 29-60 (2008). https://doi.org/10.1016/j.nuclphysa.2007.10.011
[22] D. M. William, J. S. Wladyslaw, Nuclear masses and deformations. Nucl. Phys **81**, 1-60 (1966). https://doi.org/10.1016/S0029-5582(66)80001-9
[23] A. N. Antonov, D. N. Kadrev, M. K. Gaidarov et al., Temperature dependence of the symmetry energy and neutron skins in Ni, Sn, and Pb isotopic chains. Phys. Rev. C **95**, 024314 (2017). https://doi.org/10.1103/PhysRevC.95.024314
[24] T. Naito, R. Akashi, H. Z. Liang, Application of a Coulomb energy density functional for atomic nuclei: Case studies of local density approximation and generalized gradient approximation. Phys. Rev. C **97**, 044319 (2018). https://doi.org/10.1103/PhysRevC.97.044319
[25] G. Lugones, A. G. Grunfeld, Surface and curvature properties of charged strangelets in compact objects. Phys. Rev. C **103**, 035813 (2021). https://doi.org/10.1103/PhysRevC.103.035813
[26] E. Wigner, On the Consequences of the Symmetry of the Nuclear Hamiltonian on the Spectroscopy of Nuclei. Phys. Rev **51**, 106 (1937). https://doi.org/10.1103/PhysRev.51.106
[27] R. F. Casten, Nuclear Structure from a Simple Perspective. Oxford. Acad **32**, 358-358 (2001). https://doi.org/10.1093/acprof:oso/9780198507246.001.0001
[28] G. Royer, C. Gautier, Coefficients and terms of the liquid drop model and mass formula. Phys. Rev. C **73**, 067302 (2006). https://doi.org/10.1103/PhysRevC.73.067302
[29] Z. M. Niu, H. Z. Liang, Nuclear mass predictions based on Bayesian neural network approach with pairing and shell effects. Phys. Lett. B **778**, 48-53 (2018). https://doi.org/10.1016/j.physletb.2018.01.002
[30] B. S. Cai, C. X. Yuan, Random forest-based prediction of decay modes and half-lives of superheavy nuclei. Nucl. Sci. Tech **34**, 204 (2023). https://doi.org/10.1007/s41365-023-01354-5
[31] Y. Y. Cao, J. Y. Guo, B. Zhou, Predictions of nuclear charge radii based on the convolutional neural network. Nucl. Sci. Tech **34**, 152 (2023). https://doi.org/10.1007/s41365-023-01308-x
[32] T. S. Shang, J. Li, Z. M. Niu, Prediction of nuclear charge density distribution with feedback neural network. Nucl. Sci. Tech **33**, 153 (2022). https://doi.org/10.1007/s41365-022-01140-9
[33] W. H. Ye, Y. B. Qian, H. K. Wang, Multiple constraints on nuclear mass formulas for reliable extrapolations. Phys. Rev. C **107**, 044302 (2023). https://doi.org/10.1103/PhysRevC.107.044302
[34] G. T. Garvey, W. J. Gerace, R. L. Jaffe et al., Set of Nuclear-Mass Relations and a Resultant Mass Table. Rev. Mod. Phys **41**, 1-80 (1969). https://doi.org/10.1103/RevModPhys.41.S1
[35] A. Bhagwat, Simple nuclear mass formula. Phys. Rev. C **90**, 064306 (2014). https://doi.org/10.1103/PhysRevC.90.064306
[36] M. Gong, F. Zhao, S. Y. Zeng et al., An experimental study on local and global optima of linear antenna array synthesis by using the sequential least squares programming. Appl. Soft. Comput. **148**, 110859 (2023). https://doi.org/10.1016/j.asoc.2023.110859
[37] X. Y. Xu, L. Deng, A. X. Chen et al., Improved nuclear mass formula with an additional term from the Fermi gas model. Nucl. Sci. Tech **35**, 91 (2024). https://doi.org/10.1007/s41365-024-01450-0
[38] P. Möller, J. R. Nix, Nuclear pairing models. Nucl. Phys. A **536**, 20-60 (1992). https://doi.org/10.1016/0375-9474(92)90244-E
[39] K. Lakshmi, B. Mahaboob, M. Rajaiah et al., Ordinary least squares estimation of parameters of linear model. J. Math. Comput. Sci. **11**, 2015-2030 (2021). https://doi.org/10.28919/jmcs/5454
[40] B. Rao, L. Yang, S. H. Zhong et al., Robust approximation of chance constrained optimization with polynomial perturbation. Comput. Optim. Appl. 1-27 (2024). https://doi.org/10.1007/s10589-024-00602-7
[41] F. Flachsenberg, M. Rarey, LSLOpt: An open-source implementation of the step-length controlled LSL-BFGS algorithm. J. Comput. Chem. **42**, 1095-1100 (2021). https://doi.org/10.1002/jcc.26522
[42] Y. L. Lu, W. Y. Li, C. M. Zhang et al., A Class New Hybrid Conjugate Gradient Method for Unconstrained Optimization. J. Comput. Chem. **12**, 1941-1949 (2015). https://api.semanticscholar.org/CorpusID:124611131
[43] Y. G. Pei, D. T. Zhu, On the Global Convergence of a Projective Trust Region Algorithm for Nonlinear Equality Constrained Optimization. Acta. Math. Sin.-English Ser. **34**, 1804-1828 (2018). https://doi.org/10.1007/s10114-018-7063-4
[44] P. G. Chen, Y. J. Peng, S. J. Wang, The Hessian matrix of Lagrange function. Linear. Algebra. Appl. **531**, 537-546 (2017). https://doi.org/10.1016/j.laa.2017.06.012
[45] F. S. P. S. Abad, M. Allahdadi, H. M. Nehi, Interval linear fractional programming: optimal value range of the objective function. Comp. Appl. Math **39**, 261 (2020). https://doi.org/10.1007/s40314-020-01308-2
[46] D. M. Hou, Y. X. Ning, C. Zhang, An efficient and robust Lagrange multiplier approach with a penalty term for phase-field models. J. Comput. Phys **488**, 112236 (2023). https://doi.org/10.1016/j.jcp.2023.112236
[47] P. Armand, N. N. Tran, Boundedness of the inverse of a regularized Jacobian matrix in constrained optimization and applications. Optim. Lett **16**, 2359-2371 (2022). https://doi.org/10.1007/s11590-021-01829-7
[48] Z. M. Niu, B. H. Sun, H. Z. Liang et al., Improved radial basis function approach with odd-even corrections. Phys. Rev. C **94**, 054315 (2016). https://doi.org/10.1103/PhysRevC.94.054315